Photoluminescence Quenching of Poly(3-hexylthiophene) by Carbon Nanotubes

ARTICLE *in* THE JOURNAL OF PHYSICAL CHEMISTRY C · APRIL 2012

Impact Factor: 4.77 · DOI: 10.1021/jp300115q

3 AUTHORS, INCLUDING:

Dilip K Singh
National Physical Laboratory - India
18 PUBLICATIONS **222** CITATIONS
SEE PROFILE

Parameswar K Iyer
Indian Institute of Technology Guwahati
92 PUBLICATIONS **1,463** CITATIONS
SEE PROFILE

THE JOURNAL OF PHYSICAL CHEMISTRY C

Article

pubs.acs.org/JPCC

Photoluminescence Quenching of Poly(3-hexylthiophene) by Carbon Nanotubes

Prasanta J. Goutam,[†] Dilip K. Singh,[‡] and Parameswar K. Iyer*[,†]

[†]Department of Chemistry and [‡]Center for Nanotechnology, Indian Institute of Technology Guwahati, Guwahati 781039, Assam, India

ABSTRACT: High photoluminescence quenching of poly(3-hexylthiophene) (P3HT) is observed on preparing composites with multiwalled carbon nanotubes (MWCNT) and single walled carbon nanotubes (SWCNT) even in the presence of very minor quantities of carbon nanotubes. With the experimental findings, that include results from the UV−vis spectroscopy, photoluminescence spectroscopy, and time-resolved photoluminescence spectroscopy the nature of this photoluminescence quenching mechanism has been studied and found to be static quenching. The photoluminescence quenching of P3HT by MWCNT is more efficient in comparison to SWCNT. The nature of the photoluminescence quenching has been confirmed as static quenching without any dynamic contribution.

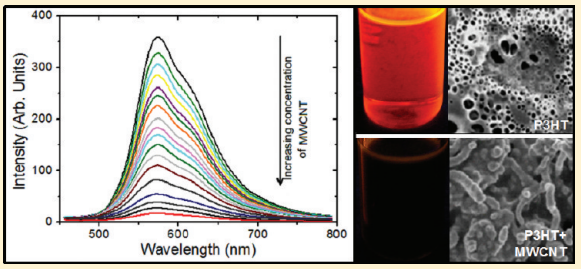

INTRODUCTION

Photoluminescence (PL) quenching has been a subject of great interest due to its potential use in many overlapping areas of material science and biomedical applications. Specific DNA/RNA detection[1] and optical oxygen/gas sensing[2] are some recent examples where the detection techniques are based on PL quenching of some fluorescent materials. Variety of molecular interactions like molecular rearrangements, excited-state reactions, energy transfer, ground-state complex formation, and collisional quenching are responsible for PL quenching.[3]

Photoluminescence measurements of conducting polymers have been used for various applications such as to study conductance switching and data-storage in polythiophene based devices.[4] In a conjugated polymer film, in situ PL measurements can be used as a probing method to read the state for memory and storage application of a device.[5] Poly(3-hexylthiophene) (P3HT)[6] is a highly fluorescent conducting polymer used as electron donor in bulk hetero junction solar cells with record power conversion efficiencies of up to 5%.[7−9] The most efficient organic photovoltaic solar cells to date utilizes a bulk hetero junction of conjugated polymer electron donor and PCBM/fullerene derivative electron acceptor with solar power conversion efficiencies of nearly 8%.[10] However, in these materials, the electron mobility depends strongly on fullerene clustering and hopping transport.[11−13] Several unique properties of carbon nanotubes have motivated their investigation as potential replacements for fullerene derivatives as the acceptor phase of devices.[14] Recent studies on blends of conjugated polymers and single walled carbon nanotubes (SWCNTs) by various groups suggest that efficient exciton quenching occurs at these interfaces.[15,16] Ionization potential and electron affinity estimates for P3HT and CNTs suggest that a type II band offset should be formed at the interface. Indeed, several spectroscopic studies on polymer-SWCNT systems have concluded that photoinduced interfacial charge separation occurs in these systems. Again, quenching of the polymer PL or a faster PL decay is often reported as an indication of photoinduced electron transfer.[17] It is well-known that fast transfer of photoinduced charges from donor to acceptor is very essential for an efficient photovoltaic device. If the electron is not transferred within few femto-seconds in the working of photovoltaic device, the photo generated exciton will decay to ground state, emitting PL and resulting in a device with poor efficiency. Hence, composites that show high PL quenching are in focus for applications in solar cell construction.[18,19] Thus, preparation of composite materials, consisting of conducting polymer donors and carbon nanomaterials as acceptor is an active area of research receiving immense attention.

Composites of P3HT with multiwalled carbon nanotube (MWCNT)[20] and SWCNT[21] are well characterized in literature. In these composites, high PL quenching of P3HT occurs even if a small amount of carbon nanomaterial is blended. In a recent report on enhancement of photostability of P3HT,[22] it was observed that very high PL quenching of P3HT solution occurred on addition of very low amount of MWCNT. However, despite this and few other observations of significant quenching behavior by CNTs, the nature of this PL quenching (static or dynamic) has not yet been reported.[23]

In this manuscript, we report about the PL quenching of P3HT by MWCNT and SWCNT and ascertained the nature of PL quenching carefully by using a combination of spectroscopic techniques.

EXPERIMENTAL SECTION

Chemicals and Solvents. P3HT used in these studies were synthesized by a known oxidative polymerization method using

Received: January 4, 2012
Revised: March 4, 2012
Published: March 20, 2012

   dx.doi.org/10.1021/jp300115q | J. Phys. Chem. C 2012, 116, 8196−8201

$FeCl_3$ as catalyst.[24] Gel permeation chromatographic analysis of the synthesized P3HT (THF, Polystyrene standard) showed weight average molecular weight, M_w = 50 439 with PDI-1.05.[25] MWCNT and SWCNT (Shenzhen Nanotech, China) were used as received. All solvents were used after purifications by standard purification techniques.[26]

Instrumentation. Field emission scanning electron microscopic (FESEM) images were recorded in a Carl Zeiss SIGMA field emission scanning electron microscope. Ultrasonication was done in a JAC Ultrasonic 1505 ultrasonicator to disperse and make uniform composites. UV−vis spectra were recorded on a PerkinElmer Lambda 25 UV−vis spectrophotometer at room temperature. PL studies were done using a Varian PL spectrophotometer. Time resolved PL spectra were recorded in a Lifespec-II, Edinburgh instruments (Model No. FSP 920).

RESULTS AND DISCUSSION

Morphological Characterization of P3HT Nanotube Composites. The MWCNT-P3HT and SWCNT-P3HT composite stock solutions were prepared using simple ultrasonication technique by sonicating it for 30 min. Concentrations of the composites were maintained in micro molar range to reduce the possibility of self-quenching effect arising due to molecular aggregation. It was observed that the original red orange color of P3HT solution turns dark brown in the composites (P3HT- MWCNT composite is shown in Figure 1).

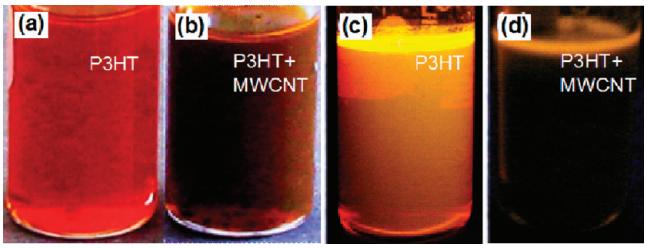

Figure 1. Photograph of chloroform solution of (a) P3HT under white light (b) P3HT-MWCNT composite under white light (c) P3HT under UV light and (d) P3HT-MWCNT composite under UV light.

Part a of Figure 2 depicts the SEM image of pristine P3HT film appearing as smooth and uniform thickness with micrometer size porous structure. Films of P3HT are well characterized in literature.[22] Pores in the dried film arise due to evaporation of solvent during solidification/film formation.

Parts b and c of Figure 2 show micrographs of pristine MWCNT and SWCNT respectively. Parts d and e of Figure 2 show the morphology of P3HT-MWCNT and P3HT-SWCNT composites respectively for maximum quenched samples. In case of P3HT-MWCNT composite, nanotubes are clearly distinguishable in the image. The diameter of MWCNTs in the composites is increased in size (~74 nm) indicating covering of the nanotube surfaces by P3HT coating. We observed photoluminescence quenching in P3HT-MWCNT composites with enhanced photostability.[22] However, in P3HT-SWCNT composites, the distinct shapes of nanotubes were not clearly seen (part e of Figure 2).

UV−vis and Photoluminescence Spectroscopy. The changes in the absorption spectra of P3HT with increasing concentration of MWCNTs are shown in part a of Figure 3. These experimental absorption curves were fitted using combination of Gaussian lineshapes to exactly determine the peak position, line width, and intensity. Part b of Figure 3 shows fitted spectra of pristine P3HT solution (i.e., before addition of MWCNTs). Two distinct peaks, with absorption maxima 373.85 nm (assigned as Peak-1) and 443.56 nm (assigned as Peak-2) respectively could be deconvoluted. Variation in the absorption maxima with increasing MWCNTs concentration in the P3HT solution is shown in part c of Figure 3. Absorption peak position is found to be monotonically blue-shifted with increasing concentration of MWCNTs. This indicates the increase in the band gap with addition of MWCNTs. More interestingly a systematic shift in the absorption peak position indicates interaction between P3HT and MWCNTs. The minor blue shifts observed for the absorption maxima of the composites are common and are in agreement with earlier reports in the literature for CNT composites with P3HT.[22,27,28] In the composites, the P3HT is wrapped over the surface of CNT and is modified from its pristine form due to the $\pi-\pi$ and CH$-\pi$ interactions with the CNTs resulting in modifications of both intrachain and interchain interactions[29,30] leading to the observed blue shift of absorption maxima in the composites. Part d of Figure 3 shows change in the absorbance of P3HT with increasing concentration of MWCNTs. Absorbance intensity of Peak-1 does not show appreciable change, whereas that of Peak-2 gets monotonically decreased.

PL intensity of P3HT is found to monotonically decrease with addition of MWCNTs (part a of Figure 4). To estimate the quenching efficiency of MWCNTs for P3HT and investigate the mechanism of PL quenching, these PL spectra were fitted using Gaussian line profile, typically shown for P3HT alone in part b of Figure 4. PL spectra of P3HT is found to consist of three peaks at wavelengths 669.0 (Peak-1), 616.5 (Peak-2), and 622.9 nm (Peak-3) (part b of Figure 4). Part c of Figure 4 shows the Stern−Volmer plot corresponding to these three components. Part d of Figure 4 shows the Stern−Volmer plot corresponding to the total intensity observed experimentally at integrated peak position. The Stern−Volmer plot follows linear behavior except at the very high concentration where it shows exponential nature. The inset of part d of Figure 4 shows the linear fit for lower concentration ranges given by $F_0/F = 1 + \alpha_1 x$, where α_1 equals to 0.0005974 ± 0.000368. The combined region could be fitted with $F_0/F = 1 + \alpha_2 x + \beta_2 \exp(\gamma_2 x)$. Where, α_2 = 0.0005974, β_2 = 0.02896 and γ_2 is 0.0005974, separate fit for lower concentration region with only linear curve shows better fit as shown in insert of part d of Figure 4.

Positive deviations from the Stern−Volmer equations have been observed when the extent of quenching is large. Such a situation is usually interpreted in terms of a "sphere of action" within which the probability of quenching is unity. The "modified form of the Stern−Volmer equation"[3] expressed by $F_0/F = (1 + K_D[Q])\exp[Q]VN/1000$ does not give a good fit in this case, where V is the volume of the sphere, representing the effective radius within which the probability of quenching is unity. This equation modifies to purely exponential growth when contribution of dynamic quenching is negligible, that is, $K_D \approx 0$.

The linear nature of Stern−Volmer plot indicates that either of the two possible mechanisms of PL quenching, static or dynamic quenching is involved in this process. Shift in the UV−vis absorption maxima indicates a strong probability of static quenching that is through the formation of nonfluorescent complex. When such a complex absorbs light, it returns to the ground state without the emission of a photon. This is further confirmed through time-resolved photoluminescence spectroscopy (TRPL).

Figure 5 shows the TRPL spectra of P3HT when excited with 475 nm diode laser and emission is monitored at 569 nm.

dx.doi.org/10.1021/jp300115q | J. Phys. Chem. C 2012, 116, 8196−8201

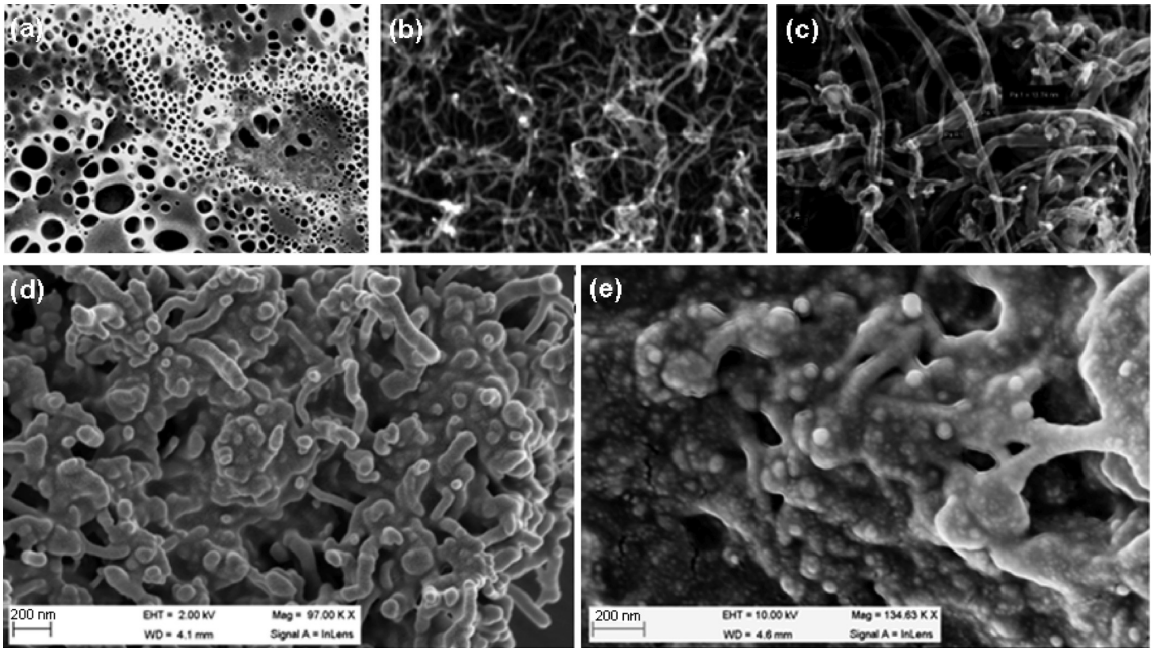

Figure 2. FESEM micrographs of (a) pristine P3HT, (b) pure MWCNT, (c) pure SWCNT, (d) P3HT-MWCNT composite, and (e) P3HT-SWCNT composite.

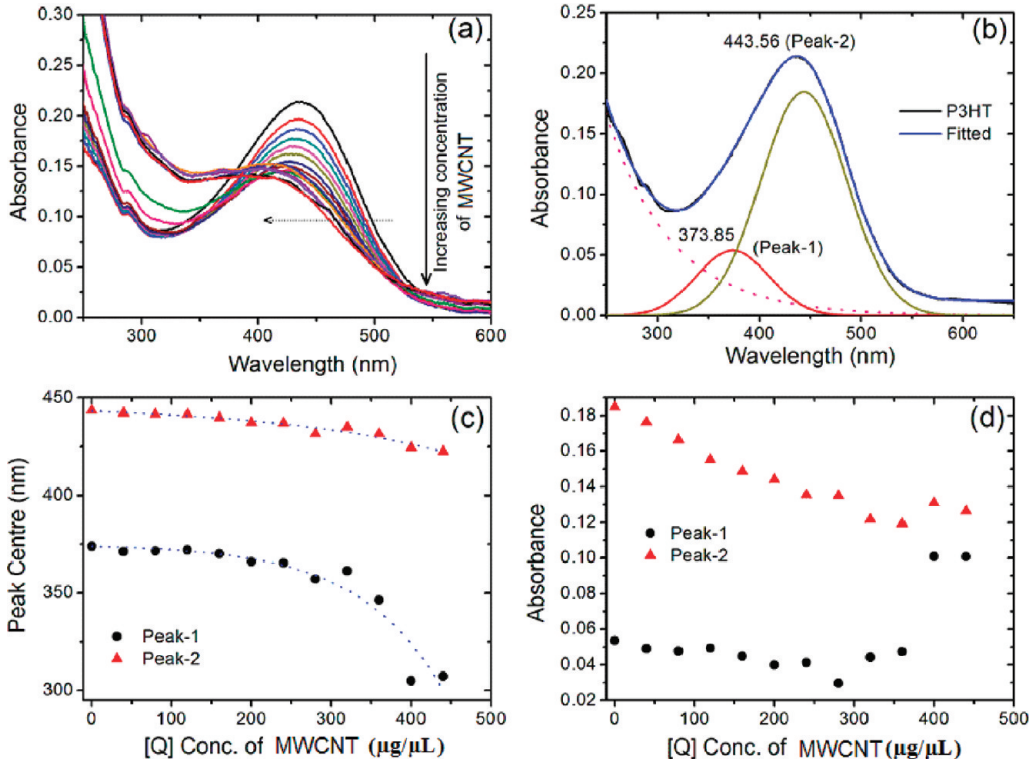

Figure 3. UV−vis spectra of (a) P3HT upon addition of MWCNT, (b) deconvoluted peaks, (c) change in peak center, and (d) changes in absorption.

With continuous addition of MWCNTs, the TRPL spectra were recorded for various concentrations of MWCNTs. Visibly all the spectra lie over one another. These spectra were deconvoluted using exponential decay profile to estimate the PL lifetime, typically shown for P3HT alone in part a of Figure 5 indicating presence of two decay channels with 140.14 ± 2.96 ns (τ_1) and 555.97 ± 1.86 ns (τ_2) responsible for 25.12 and 74.88% of the decay process respectively. Parts b and c of Figure 5 show the variation in (τ_0/τ) for the decay channels τ_1 and τ_2 respectively with increasing concentration of MWCNTs. This figure clearly shows that ratio of PL decay time before and after addition of MWCNTs remains constant nearly at 1. This eradicates any possibility of existence of dynamic quenching contribution, since such process would lead to decrease in the PL excited state lifetime. These TRPL results are in agreement with linear Stern−Volmer plot and peak position shift observed

dx.doi.org/10.1021/jp300115q | J. Phys. Chem. C 2012, 116, 8196−8201

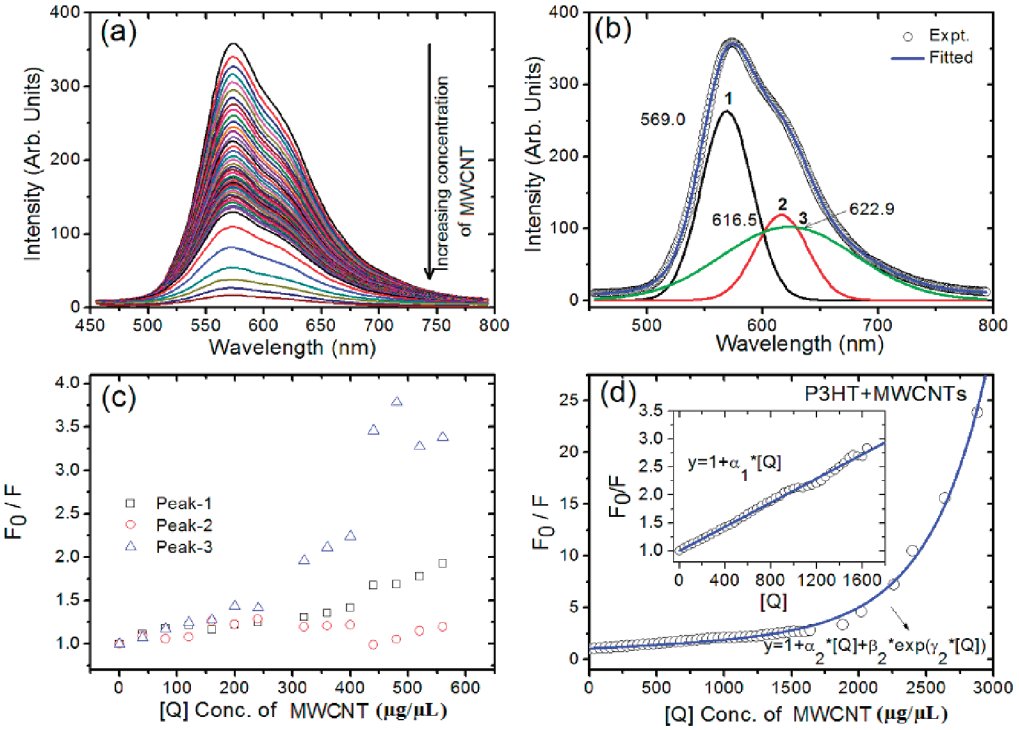

Figure 4. Photoluminescence quenching of P3HT upon addition of MWCNT (a), deconvoluted peaks (b), F_0/F for the three peaks at different concentrations and Stern–Volmer plot (d).

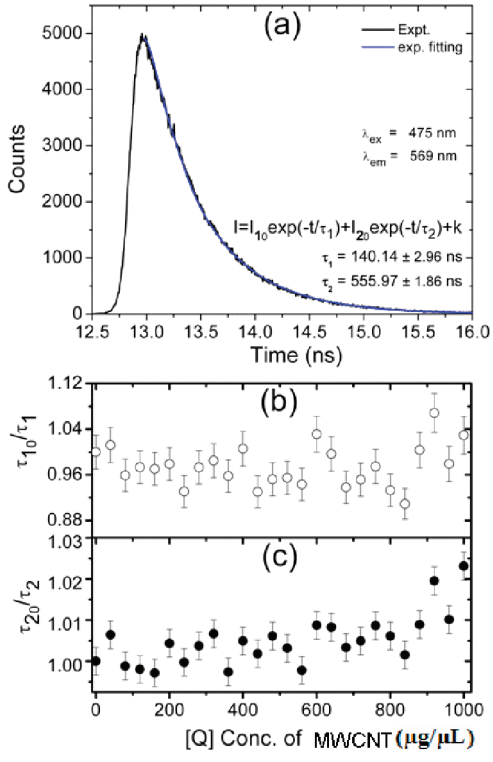

Figure 5. (a) Typical Time resolved photoluminescence spectra (TRPL) of P3HT showing two exponential decay times τ_1 = 140.14 ± 2.96 ns and τ_2 = 555.97 ± 1.86 ns. Variation in the relative decay lifetime of (b) τ_1 = 140.14 ± 2.96 ns and (c) τ_2 = 555.97 ± 1.86 ns components with addition of MWCNTs shows $\tau_{10}/\tau_1 \sim 1$ and $\tau_{20}/\tau_2 \sim 1$ representing static quenching.

in the absorption spectra indicates static quenching to be only responsible for the process.

Further, experiments have been carried out with SWCNTs to estimate the relative quenching efficiency of MWCNTs and SWCNTs. Part a of Figure 6 shows the change in the UV–vis absorption spectra with increasing concentration of SWCNTs. Unlike MWCNTs, visibly little change in the absorption spectra appears with addition of SWCNTs. Similar to the MWCNTs, these spectra were deconvoluted using a combination of two Gaussian peaks. The variation in the peak position and intensity of these two components are shown in parts b–e of Figure 6. Similar to MWCNTs, with addition of SWCNTs to P3HT the absorption maximum monotonically shifts to the lower wavelengths. But in case of SWCNTs, change is relatively weak and follows a linear trend for the similar concentration. In case of SWCNTs, the absorbance do not show appreciable change in comparison to MWCNTs as shown in parts d and e of Figure 6 respectively for peak-1 and peak-2. This observation is supported by literature report where absorption spectra of the P3HT-SWCNT did not change significantly upon addition of SWCNT indicating insufficient interaction between the two materials.[31]

Part a of Figure 7 shows the change in the PL spectra of P3HT with increasing concentration of SWCNTs. Corresponding Stern–Volmer plot is shown in part b of Figure 7. Stern–Volmer plot is linear for lower concentration and shows positive curvature at higher concentrations. Nonlinear curvature may arise either due to a number of factors like combined effect of static and dynamic quenching, limited accessibility of quenchers or due to very large extent of quenching. Presence of dynamic quenching in our case is eliminated through time-resolved studies presented later, whereas the limited accessibility of quenchers to the nanotubes due to bundling effect would lead to negative curvature in contrast to the observed upward curvature. Such positive curvature behavior of Stern–Volmer plot has been observed in case of quenching of fluorescein by SWCNTs due to enhanced dipole–dipole

dx.doi.org/10.1021/jp300115q | J. Phys. Chem. C 2012, 116, 8196–8201

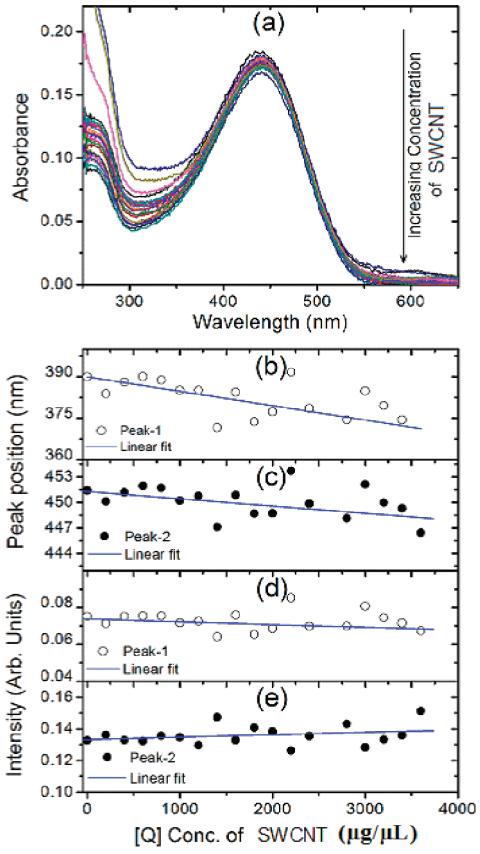

Figure 6. UV−vis absorption studies of P3HT SWCNT nanocomposites. (a) Variation of absorption peak maxima with increasing concentration of SWCNTs, (b) and (c) show change in the absorption maxima of components peak-1 and peak-2, (d) and (e) shows variation in the absorption intensity with increasing SWCNT concentration.

energy transfer in presence of structural defects. Such behavior is expressed as compressed exponential.[32] Similar to the above experiments with MWCNTs, on continuous addition of SWCNTs to P3HT at various concentrations, the change in the PL lifetime has been monitored carefully.

These spectra were fitted with a combination of two exponential decay components. The change in the decay time for these two components τ_1 and τ_2 are shown in parts a and b of Figure 8, respectively. The ratios τ_{10}/τ_1 and τ_{20}/τ_2 remain nearly constant at 1. This strongly indicates the absence of any contribution from dynamic quenching. Thus, the positive deviation observed in Stern−Volmer plot arises from large extent of quenching explained by 'Sphere of action model' due to extended cylindrical geometry of nanotubes as compared to spherical representing large action area.

Possibility of existence of FRET is eliminated considering the strong absorption peak maxima shift of P3HT observed upon addition of MWCNTs. Such peak shift can only occur upon molecular complex formation, an essential condition required for static quenching mechanism. The actual nature of interactions between various fluorophores and CNTs has remained unclear. In a recent report, it was mentioned that there is no peak shift in case of energy transfer from nile blue A to CNTs though FRET mechanism and dynamic quenching process was accounted to play a major role.[33] In this process, neither a chemical alteration nor complex formation takes place and hence they did not observe any absorption peak shift of nile

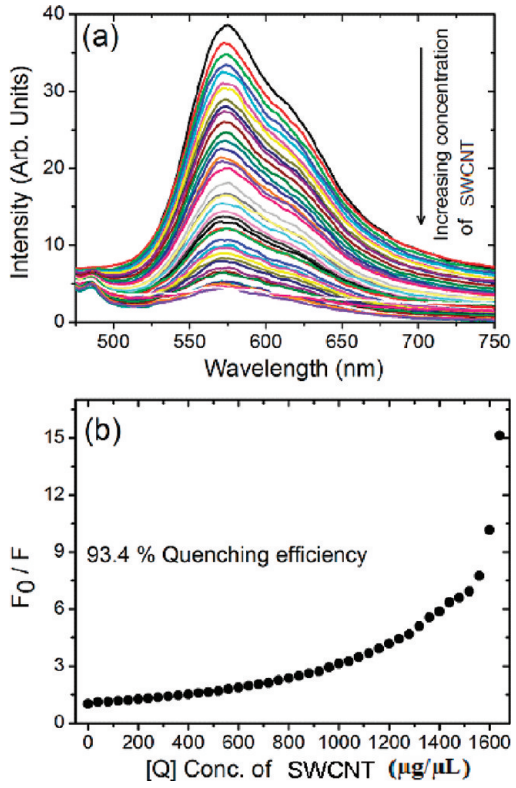

Figure 7. Photoluminescence quenching of P3HT upon addition of (a) SWCNT and (b) Stern−Volmer plot.

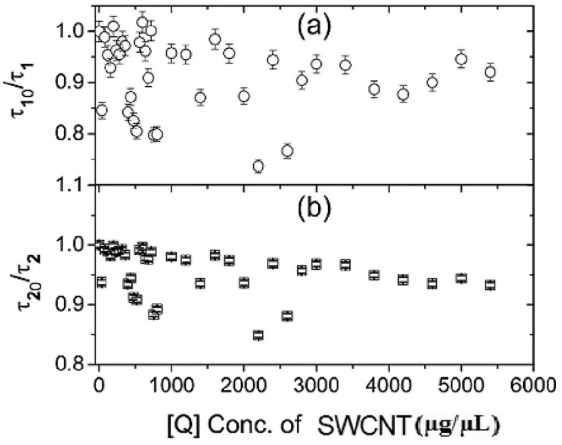

Figure 8. Variation in the lifetime ratio of P3HT before and after addition of SWCNTs with increasing concentration of SWCNT.

blue A. This is contrary to our observations of absorption peak shift indicating static quenching to be dominant process in the quenching of P3HT. In contrast, in the case of rhodamine B, static quenching mechanism has been reported by CNTs.[34] Our experiments show that "static quenching", the mechanism of photoluminescence quenching of P3HT by carbon nanotubes is different from the "dynamic quenching mechanism" reported for photoluminescence quenching of quantum dots by carbon nanotubes.[23] It is, however, not clear what factors decide the dominance of one mechanism over another for the two different mechanisms reported: dynamic[33] and static[34] quenching processes. Further, MWCNTs do not possess any distinct energy bandgap to overlap with the emission band of P3HT for dipolar energy transfer popularly known as FRET.

dx.doi.org/10.1021/jp300115q | J. Phys. Chem. C 2012, 116, 8196−8201

Interestingly, in case of SWCNTs we did not observe such strong peak shift, although it possesses distinct band gaps required for FRET to occur. It was not possible to monitor changes in the absorption peak intensity of CNTs due to very low concentration of CNTs and absence of distinct absorption bands of MWCNTs. In agreement with spectroscopic studies, morphological study of composite[22] using FESEM and TEM shows P3HT wrapping on the surface of CNT indicating involvement of static quenching, contrary to the FRET which occurs at certain distances through energy exchange between radiating dipoles due to long-range dipole−dipole interactions.

CONCLUSIONS

From the experimental results comprising UV−vis and photoluminescence spectroscopic studies, the nature of photoluminescence quenching observed in P3HT and carbon nanotube composites are confirmed to be "static quenching". Positive deviation observed in Stern−Volmer plot arises from large extent of quenching to be explained using "Sphere of action model". The effect of photoluminescence quenching of P3HT by MWCNT is more in comparison to SWCNT. Our results establish that the nature of photoluminescence quenching of P3HT by carbon nanotubes is static without any dynamic contribution. Understanding the PL quenching mechanism of P3HT by carbon based nanomaterials is important since they provide valuable insights into the photoinduced electron transfer processes between donor and acceptor materials in photovoltaic devices that are responsible for improved efficiencies.

AUTHOR INFORMATION

Corresponding Author

*E-mail: pki@iitg.ernet.in, phone: +91-361-258-2314, fax: +91-361-258-2349.

Notes

The authors declare no competing financial interest.

ACKNOWLEDGMENTS

We thank the Department of Science and Technology (DST) (No. SR/S1/PC-02/2009, DST/TSG/PT/2009/11 and DST/TSG/PT/2009/23) for financial support. The Central Instruments Facility, IIT Guwahati, is acknowledged for providing electron microscopic facilities. P.J.G. and D.K.S. thank CSIR for Senior Research Fellowship.

REFERENCES

(1) Kurata, S.; Kanagawa, T.; Yamada, K.; Torimura, M.; Yokomaku, T.; Kamagata, Y.; Kurane, R. *Nucleic Acid Res.* **2001**, *29* (6), 1−5.
(2) Anni, M.; Rella, R. *J. Phys. Chem. B* **2010**, *114*, 1559−1561.
(3) Lakowicz, J. R. *Principles of fluorescence spectroscopy*, Third ed.; Springer: New York, 2006.
(4) Botta, C.; Mercogliano, C.; Bolognesi, A.; Majumdar, H. S.; Pal, A. J. *Appl. Phys. Lett.* **2004**, *85*, 2393−2395.
(5) Majumdara, H. S.; Bottab, C.; Bolognesib, A.; Pal, A. J. *Synth. Met.* **2005**, *148*, 175−178.
(6) McCullough, R. D. *Adv. Mater.* **1998**, *10*, 93−116.
(7) Chirvaze, D.; Chiguvare, Z.; Knipper, M.; Parisi, J.; Dyakonov, V.; Hummelen, J. C. *J. Appl. Phys.* **2003**, *93*, 3376−3383.
(8) Chirvase, D.; Parisi, J.; Hummelen, J. C.; Dyakonov, V. *Nanotechnology* **2004**, *15*, 1314−1317.
(9) Günes, S.; Neugebauer, H.; Sariciftci, N. S. *Chem. Rev.* **2007**, *107*, 1324−1338.
(10) Koster, L. J. A.; Mihailetchi, V. D.; Bloom, P. W. *Appl. Phys. Lett.* **2006**, *88*, 93511−93513.
(11) Liang, Y.; Xu, Z.; Xia, J.; Tsai, S. T.; Wu, Y.; Li, G.; Ray, C.; Yu, L. *Adv. Mater.* **2010**, *22*, E−135-E138.
(12) Green, M. A.; Emery, K.; Hishikawa, Y.; Warta, W. *Prog. Photovolt: Res. Appl.* **2010**, *18*, 346−352.
(13) Grzegorczyk, W. J.; Savenije, T. J.; Dykstra, T. E.; Piris, J.; Schins, J. M.; Siebbeles, L. D. *J. Phys. Chem. C* **2010**, *114*, 5182−5186.
(14) Sgobba, V.; Guldi, D. M. *J. Mater. Chem.* **2008**, *18*, 153−157.
(15) Imin, P.; Cheng, F.; Adronov, A. *Polym. Chem.* **2011**, *2*, 411−416.
(16) Holt, J. M.; Ferguson, A. J.; Kopidakis, N.; Larsen, B. A.; Bult, J.; Rumbles, G.; Blackburn, J. L. *Nano Lett.* **2010**, *10*, 4627−4633.
(17) Ferguson, A. J.; Blackburn, J. L.; Holt, J. M.; Kopidakis, N.; Tenent, R. C.; Barnes, T. M.; Heben, M, J.; Rumbles, G. *J. Phys. Chem. Lett.* **2010**, *1*, 2406−2411.
(18) Wong, W. Y.; Zhuwang, X.; He, Z.; Djuri, A. B.; Yip, C. T.; Cheung, K. Y.; Haiwang; Mak, C. S. K.; Chan, W. K. *Nature Mat.* **2007**, *6*, 521−527.
(19) Kuila, B. K.; Park, K.; Dai, L. *Macromolecules* **2010**, *43*, 6699−6705.
(20) Kuila, B. K.; Malik, S.; Batabyal, S. K.; Nandi, A. K. *Macromolecules* **2007**, *40*, 278−287.
(21) Zhang, Z. B.; Li, J.; Qu, M.; Cabezas, A. L.; Zhang, S. L. *IEEE Electron Device Lett.* **2009**, *30* (12), 1302−1304.
(22) Goutam, P. J.; Singh, D. K.; Giri, P. K.; Iyer, P. K. *J. Phys. Chem. B* **2011**, *115*, 919−924.
(23) Pan, B.; Cui, D.; Ozkan, C. S.; Ozkan, M.; Xu, P.; Huang, T.; Liu, F.; Chen, H.; Li, Q.; He, R.; Gao, F. *J. Phys. Chem. C* **2008**, *112*, 939−944.
(24) Pomerantz, M.; Liu, L.; Zhang, X. *Arkivoc* **2003**, *12*, 119−137.
(25) Reddy, P. K.; Goutam, P. J.; Singh, D. K.; Ghoshal, A. K.; Iyer, P. K. *Polym. Degrad. Stab.* **2009**, *94*, 1839−1848.
(26) Armarego, W. L. F.; Perrin, D. D. *Purification of Laboratory Chemicals*; Butterworth-Heinemann: Burlington, MA, 2002.
(27) Kuila, B. K.; Nandi, A. K. *Macromolecules* **2004**, *37*, 8577−8584.
(28) Kuila, B. K.; Nandi, A. K. *J. Phys. Chem. B* **2006**, *110*, 1621−1631.
(29) Rughooputh, S. D. D. V.; Hotta, S.; Heeger, A. J.; Wudl, F. *J. Polym. Sci., Part B: Polym. Phys.* **1987**, 1071−1078.
(30) Malik, S.; Jana, T.; Nandi, A. K. *Macromolecules* **2001**, *34*, 275−282.
(31) Kymakis, E.; Amaratunga, G. A. J. *Synth. Met.* **2004**, *142*, 161−167.
(32) Singh, D. K.; Giri, P. K.; Iyer, P. K. *J. Phys. Chem. C* **2011**, *115*, 24067−24072.
(33) Ahmad, A.; Kern, K.; Balasubramanian, K. *ChemPhysChem.* **2009**, *10*, 905−909.
(34) Ahmad, A.; Kurkina, T.; Kern, K.; Balasubramanian, K. *ChemPhysChem.* **2009**, *10*, 2251−2255.